Microfluid Nanofluid (2012) 13:421–428
DOI 10.1007/s10404-012-0970-2

RESEARCH PAPER

Numerical simulation of traveling wave-induced electroconvection

Sebastian Schmidt · Arnulf Latz

Received: 12 September 2011 / Accepted: 21 November 2011 / Published online: 30 March 2012

Abstract A method is presented for simulating the convection in fluid flows induced by high frequency electric fields typical, e.g. for electrohydrodynamic pumping in microchannels. Time scale separation between electric field frequency and hydrodynamic flow scales is explicitly taken into account in the derivation of the model. A finite volume numerical scheme is presented which resolves the problem three dimensionally in space. The method is checked against experimental findings.

Keywords Electrohydrodynamics · Microfluidic · Traveling waves

1 Introduction

In this work, we present a method for simulating the convection in fluid flows induced by high frequency electric fields. Our work is motivated by electrohydrodynamic (EHD) pumping technologies in lab-on-chip applications as described in Sect. 2. The extended potential of the method presented here was shown in (Böttcher et al. 2011), where a full simulation of EHD pumping in comparison with a complex filtration experiment has been carried out in collaboration with the authors without presentation of the actual derivation of the method in both modeling and numerics. In this paper, we derive the set of model equations in Sect. 3 and present a numerical method for solving these equations in Sect. 4. For validation purposes, we compare our results with the analytically approximable experimental results of (Melcher 1967) in Sect. 5.

Many papers dealing with the interaction of high frequency electric fields with fluid flows consider quasi one-dimensional settings or simplified two-dimensional geometries. The interaction between the electric fields and the flow is sometimes represented by a Coulomb force term (Ramos et al. 1998) $\mathbf{f} = \rho_e \mathbf{E}$ and sometimes via an electric stress tensor (Melcher 1967) $T_{ij} = \varepsilon E_i E_j - \frac{1}{2}\delta_{ij} E^2$. To eliminate any modeling ambiguity, we present a thermodynamically consistent rederivation of the relevant electrohydrodynamic equations starting from the most general set of equations for electric and hydrodynamic fields.

The full simulation of EHD pumping has also been approached recently by Iverson et al. (2009). Our method differs significantly from their approach, which does not make use of the time scale separation between hydrodynamic and electrodynamic variables. It is, therefore, not applicable for high frequency pumping, since the numerical time scale has to be smaller than the inverse of the highest frequency scale, which is much too small for any feasible flow simulation. A simulation of induced flow and electric fields is in (Iverson et al. 2009) only possible, if the time scale for changes in the electric field, i.e. the traveling wave frequency corresponds to the hydrodynamic time scale set by the flow speed and the dimension of the geometry. In our approach, the resulting forces on the fluid are averaged over the time scale set by the inverse frequency of the applied ac-electric field. The time scale for the resulting effective equations is, therefore, only the hydrodynamic scale and the numerical time scale for these equations is not bounded by the frequency scale of the electric field.

S. Schmidt (✉) · A. Latz
Fraunhofer Institute for Industrial Mathematics,
Fraunhofer Platz 1, 67663 Kaiserslautern, Germany
e-mail: sebastian.schmidt@itwm.fraunhofer.de

2 Traveling wave-based electrohydrodynamic pumping

High frequency alternating electric fields have long been used to transport fluids and suspended particles through microchannels (Fuhr et al. 1992; Green et al. 2000). For transporting particles under the influence of electric fields, one has to distinguish between applications where inhomogeneous electric fields exert a force directly on the particles by inducing an effective dipole moment in the particles (dielectrophoresis) (Ramos et al. 1998) and applications where one tries to induce an effective force on the liquid only, to avoid potentially harmful stresses on the particles (Fuhr et al. 1992, 1994). This can be achieved, e.g. by matching the frequency-dependent dielectric constant of the liquid and the particles. Two major different forces, electrothermal and electroosmotic forces (Ramos et al. 1998), can cause fluid flow in channels. Electrothermal forces are related to variations of either the dielectric function or the conductivity of the liquid over the width of the flow channel, e.g. due to induced temperature fields (Felten et al. 2006) or other effects like gradients in the salt concentration if electrolytes are used as liquids. Electroosmotic forces are due to the force on the electric double layer formed close to the electrodes (Green et al. 2002). Due to the much smaller spatial scale λ_D of the double layer (λ_D is usually in the order of a few nanometers in liquids) and the width d of the considered channels ($100\,\mu m \lesssim d \lesssim 10\,cm$), the frequency scale of ac-electroosmosis is by a factor λ_D/d smaller compared to electrothermal flow. We will concentrate on flows induced by spatial gradients of the dielectric function or the electrical conductivity across the flow channel, although the theory is also applicable to ac-electroosmosis. We will point out in Sect. 3 the terms which give rise to each of the two effects, respectively. Only recently local flow phenomena such as vortices or locally high velocities have attracted attention (Green et al. 2002; Felten et al. 2008; Böttcher et al. 2011) for these applications.

The experimental method described in Böttcher et al. (2011) allows transport of a large range of particle concentrations down to very low concentrations. A scheme of the apparatus is depicted in Fig. 1. To investigate the flow locally around the electrode area without any restriction on the shape of the electrodes, a method is needed to spatially resolve the three-dimensional flow phenomena induced by high frequency electric fields in great detail. For the water used in (Böttcher et al. 2011) and the involved flow speeds and electric field frequencies, the time scales of electric and flow field are separated by several orders of magnitude. Therefore, a time-averaging ansatz like the one we will present in the following section is necessary to obtain numerical results for the fluid flow.

3 Derivation of the equations

We will use the hydrodynamic theory of electromagnetic fields in continuous media (Landau 1984; Liu 1993) to derive the equations for the description of traveling wave phenomena. We begin with the Maxwell equations for the displacement **D**, the electric field **E** and the two magnetic fields **B** and **H**.

$$\nabla \mathbf{B} = 0 \, \nabla \mathbf{D} = \rho_e \tag{1}$$

$$\frac{\partial \mathbf{B}}{\partial t} = -\nabla \times \mathbf{E} \, \frac{\partial \mathbf{D}}{\partial t} = \nabla \times \mathbf{H} - j_e \tag{2}$$

Here ρ_e and $\mathbf{j}_e$ are the charge density and density of electric current, respectively. The equations for the standard traveling wave induced flow are derived under a few constraining assumptions. First of all, the relation between **E** and **D** as well as between **B** and **H** is assumed to be linear and quasi static

$$\mathbf{D} = \varepsilon_0 \varepsilon \mathbf{E} \tag{3}$$

$$\mathbf{B} = \mu_0 \mu \mathbf{H}, \tag{4}$$

i.e the dielectric function ε and the the magnetic permeability μ may be frequency dependent but change only slightly in the frequency range of the traveling wave. Hence, there should not be any dielectric resonances for the frequency under consideration. This sets an upper bound for the allowed frequencies depending on the liquid used. The frequencies in traveling wave applications are mostly below the MHz regime. Water solutions and the oil considered in this paper do not have resonances in this regime. Spatial variation of ε (e.g. induced by temperature variations) is allowed and is the cause for electrothermal pumping. In all applications of the traveling wave technology, the frequency ω of the wave is much smaller than c/λ, where c and λ are the vacuum speed of light and the typical wavelength of the wave, which is imposed by the construction of the electrodes as, e.g. in Fig. 1 and the condition

$$\Phi_c(\mathbf{x}) = \Phi_0^c(\mathbf{r}) \cos(\mathbf{k} \cdot \mathbf{r}), \quad \Phi_s(\mathbf{x}) = \Phi_0^s(\mathbf{r}) \sin(\mathbf{k} \cdot \mathbf{r}). \tag{5}$$

Here Φ_0^s and Φ_0^s are the amplitudes of respective voltage contributions, **k** the wave vector in the two-dimensional manifold of the electrodes and **r** a vector for a position in the manifold of the electrodes. Therefore, a transversal propagating solution of the Maxwell equations is excluded by the traveling wave boundary conditions.

In a more formal way, this can be seen by expressing the magnetic field **B** and the electric field **E** in the standard way by the electric potential Φ and the vector potential **A**

$$\mathbf{B} = \nabla \times \mathbf{A} \tag{6}$$

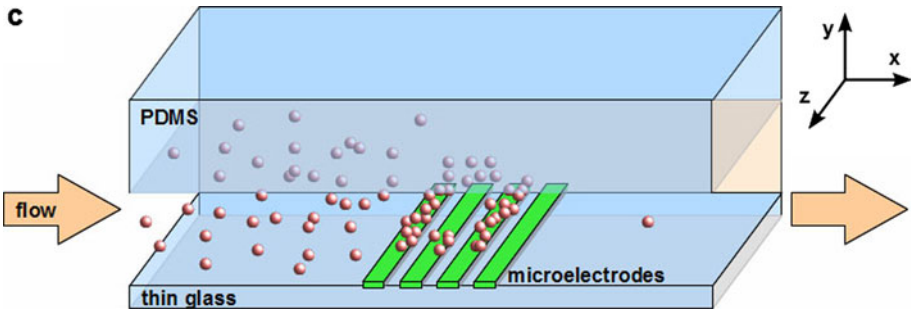

Fig. 1 Scheme of the setup of the motivating EHD-pumping device showing a possible particle aggregation above the electrodes. These induce the high frequency electric field that in turn causes three-dimensional local flow phenomena

$$\mathbf{E} = -\nabla\Phi(r,t) - \partial_t\mathbf{A} \tag{7}$$

To describe electrohydrodynamic pumping of neutral liquids in channels with traveling waves it is sufficient to choose (Melcher 1966)

$$\mathbf{j}_e = \sigma\mathbf{E} \tag{8}$$

as the constitutive relation for the electric current. Here σ is, in general, a spatially varying electric conductivity. An additional convective contribution to the electric current can be neglected in traveling wave applications for electrically neutral liquids (Melcher 1966). Replacing Eqs. (3)–(7) and (8) in (2) and using Coulomb gauge $(\nabla\cdot\mathbf{A}=0)$ we obtain

$$-\frac{\nabla^2\mathbf{A}}{\mu_0\mu} = -\varepsilon_0\varepsilon\partial_{tt}\mathbf{A} - \sigma\partial_t\mathbf{A} - \sigma\nabla\Phi - \varepsilon_0\varepsilon\nabla\partial_t\Phi \tag{9}$$

To evaluate the relative importance of the various terms, it is useful to rescale the equations using the natural units of the problem. The wavelength λ and frequency ω of the traveling wave are imposed by the construction of the external electrodes. An additional important scale is the lateral dimension d of the channels used in traveling wave applications, since they determine the order of the gradients of electromagnetic fields orthogonal to the boundaries of the channel. Let us define the spatial scale δ as the maximum of these two scales

$$\delta = \max(\lambda, d) \tag{10}$$

The product

$$c_\omega = \omega\delta \tag{11}$$

defines the velocity scale of the traveling wave. Although there is a wide range of frequencies and wavelengths used (Ramos et al. 1998; Green et al. 2000; Böttcher et al. 2011; Fuhr et al. 1992), in all applications of traveling wave technology, the relation

$$c_\omega \ll c \tag{12}$$

is fulfilled. Here, the relation $c^2 = \frac{1}{\varepsilon_0\mu_0}$ for the vacuum speed of light was used. Another important velocity scale can be derived from the electric conductivity σ by the definition

$$c_\sigma = \frac{\sigma\delta}{\varepsilon_0} \tag{13}$$

For the oil used in the experimental comparison (Sect. 5) in this paper, c_σ is of the order of $10\cdot\delta$ where δ is measured in meters. For water, it is of the order of $10^4\cdot\delta$. Even for electrolytic solutions in microchannels (i.e. $\delta \le 10^{-3}$ m), where c_σ can reach values of $\approx 10^8\cdot\delta$, the relation

$$c_\sigma \ll c \tag{14}$$

is fulfilled. Rescaling Eq. (9) and using the definitions $\hat{\Phi} := \frac{\Phi}{\delta}, \hat{\mathbf{A}} := \omega\mathbf{A}$ we obtain

$$\hat{\nabla}^2\hat{\mathbf{A}} = \frac{{c_\omega}^2}{c^2}\varepsilon\mu\hat{\partial}_{tt}\hat{\mathbf{A}} + \frac{c_\sigma c_\omega\mu}{c^2}\hat{\partial}_t\hat{\mathbf{A}} + \frac{c_\sigma c_\omega\mu}{c^2}\hat{\nabla}\hat{\Phi} + \frac{c_\omega^2}{c^2}\varepsilon\mu\hat{\nabla}\hat{\partial}_t\hat{\Phi}. \tag{15}$$

Due to (12) and (14) the right hand side of (15) is much smaller than the left hand side. Therefore in leading order, a two-scale solution is possible. The magnetic field is obtained by setting in leading order the right hand side of (15) to zero and applying the curl operator to obtain

$$\nabla^2\mathbf{H} = 0. \tag{16}$$

Since there are no macroscopic electric currents in neutral liquids this static equation is solved by $\mathbf{H} = 0$ and $\mathbf{A} = 0$. Using this solution in the right hand side of (15) and applying in addition the gradient operator, we arrive finally at a scalar equation for the potential

$$0 = -\nabla(\sigma\nabla\Phi) - \nabla(\varepsilon_0\varepsilon\nabla\partial_t\Phi) \tag{17}$$

To gain a better understanding of this equation, we rewrite it as

$$\partial_t\rho_e + \frac{\sigma}{\varepsilon\varepsilon_0}\rho_e = -\nabla\sigma\cdot\nabla\Phi - \varepsilon_0\nabla_\varepsilon\cdot\partial_t\nabla\Phi \tag{18}$$

$$\varepsilon_0\nabla\cdot(\varepsilon\nabla\Phi) = \rho_e. \tag{19}$$

If the dielectric function ε and conductivity σ are spatially constant, the right hand side of equation (18) vanishes and we obtain formally the solution

$$\rho_e = \rho_e^0\exp\left(-\frac{\sigma}{\varepsilon\varepsilon_0}t\right) \tag{20}$$

$$\nabla^2 \Phi = \frac{\rho_e^0}{\varepsilon \varepsilon_0}. \tag{21}$$

This set of equations has nonzero solutions only close to electrodes within a range of the Debye screening length λ_D, i.e. a few nanometers for the liquids under consideration. To obtain explicit solutions, the equations have to be extended by a theory of the electric double layer (Russel et al. 1989). In this way, a theory for electroosmosis can be obtained (Green et al. 2002).

We will consider the case of spatially varying dielectric function ε and/or electric conductivity σ. The range of spatial variation is set by the thickness of the channel. In most applications, this will be in the range above about 100 µm and below 10 cm, but we want to emphasize the limits of the theory are given only by Eqs. (12) and (14). The spatial gradients of ε and σ on the right hand side of (18) act as a source for the spatial variation of the electrical potential and allow for nonzero solutions of the potential.

Due to (16) and the traveling wave boundary conditions, the vector potential and thus the magnetic fields will be set to zero in the following considerations. Only the time averaged electric force will play a role. Thus, the derivation of the electrohydrodynamic equations is considerably simplified compared to the more general framework described in (Liu 1993; Jiang 1996).

The equation for the component ρu_i of the momentum density $\rho \mathbf{u}$ is given by

$$\partial_t(\rho u_i) + \partial_j(\rho u_i u_j) = \partial_j(\pi_{ij}). \tag{22}$$

For the derivation of the effective electric force in the electrohydrodynamic equations, it is sufficient to consider pressure, electric fields and viscous dissipative contribution to the stress. Using the formalism of Liu (1993) and Jiang (1996), we can write for the components π_{ij} of the stress tensor

$$\pi_{ij} = (-p - \mathbf{ED} - U)\delta_{ij} + \frac{1}{2}(E_i D_j + E_j D_i) + \eta(\partial_i v_j + \partial_j v_i) \tag{23}$$

The differential of the energy U is given by

$$dU = E_i dD_i. \tag{24}$$

Using (1), the force density $\partial_j \pi_{ij}$ can be transformed to

$$\partial_j \pi_{ij} = -\partial_i p - (\mathbf{D} \times \nabla \times \mathbf{E})_i + \rho_e E_i + \partial_j(\eta \partial_j v_i) + \partial_j(\eta \partial_i v_j). \tag{25}$$

For incompressible Newtonian flow, i.e $\nabla \cdot \mathbf{v} = 0$ and constant viscosity η, Eq. (25) can further be simplified using (2) and $\dot{\mathbf{B}} = 0$

$$\partial_j \pi_{ij} = -\partial_i p + \rho_e E_i + \eta \partial_j^2 v_i \tag{26}$$

To obtain the average velocity field, we introduce for time-dependent functions $f(t)$ a moving average $\langle f(t) \rangle^t$ defined by

$$\langle f(t) \rangle^t = \frac{1}{T} \int_t^{t+T} f(t') \mathrm{d}t'. \tag{27}$$

Here the $T = 2\ \pi/\omega$ is the time for one cycle of the traveling wave. If we decompose the velocity $\mathbf{v}$ in an averaged and a fluctuation component

$$\mathbf{v} = \mathbf{u}(t) + \mathbf{u}_c(\mathbf{r})\cos(\omega t) + \mathbf{u}_s(\mathbf{r})\sin(\omega t), \tag{28}$$

the time averaged Navier–Stokes equation is given by

$$\partial_t(\rho u_i) + \partial_j(\rho u_i u_j) = -\partial_i p + \langle \rho_e E_i \rangle^t + \eta \partial_j^2 u_i. \tag{29a}$$

$$\nabla \cdot \mathbf{u} = 0. \tag{29b}$$

The convective term in the momentum equation contains after time averaging terms quadratic in u_c and u_s. But these terms can be cancelled by an additional static pressure which has to be introduced to preserve the incompressibility also for the velocity fluctuations. The additional equations to be solved are

$$\partial_j(\rho u_{c,i} u_{c,j}) = -\partial_i p_c \tag{30a}$$

$$\partial_j(\rho u_{s,i} u_{s,j}) = -\partial_i p_c \tag{30b}$$

$$\nabla \cdot \mathbf{u}_c = 0 \tag{30c}$$

$$\nabla \cdot \mathbf{u}_s = 0. \tag{30d}$$

As a next step, we need the equation for the electric force density $\mathbf{f} = \langle \rho_e \mathbf{E} \rangle^t$. For numerical purposes, it is more convenient to use a real representation of $\Phi(r,t)$ i.e.

$$\Phi(r,t) = \Phi_c(r)\cos(\omega t) + \Phi_{\mathbf{s}}(r)\sin(\omega t). \tag{31}$$

With this ansatz we obtain from Eq. (17) a coupled set of equations for $\Phi_c(r)$ and $\Phi_s(r)$

$$\partial_i \left[\begin{pmatrix} -\varepsilon\omega & \sigma \\ \sigma & \varepsilon\omega \end{pmatrix} \begin{pmatrix} \partial_i \Phi_c \\ \partial_i \Phi_s \end{pmatrix} \right] = 0. \tag{32}$$

With the help of Φ_c and Φ_s the average electric force density $\mathbf{f}$ can be written in the form

$$\mathbf{f} = \frac{1}{2}(\nabla \cdot (\varepsilon \nabla \Phi_c))\ \nabla \Phi_c + (\nabla \cdot (\varepsilon \nabla \Phi_s))\ \nabla \Phi_s). \tag{33}$$

In electrothermal applications, the spatial dependence is due to the temperature dependence of the dielectric function or the conductivity. Therefore, in addition to the electrohydrodynamic Navier–Stokes equations (29a, 29b), the heat equation is to be solved to obtain a complete description of processes in the micro channel. As for the Navier–Stokes equations, we only have to consider the short time averaged equation and can neglect the magnetic distributions as heat sources.

$$\frac{\partial c_p \rho T}{\partial t} + \nabla(\mathbf{u} c_P \rho T) = \nabla(\lambda \nabla T) + \langle \sigma(T) \mathbf{E}^2 \rangle. \tag{34}$$

The average Joule heating term is given by

$$\langle \sigma(T)\mathbf{E}^2 \rangle = \sigma(T)\frac{1}{2}((\nabla \Phi_c)^2 + (\nabla \Phi_s)^2). \quad (35)$$

4 Numerical simulation

The numerical simulation of the interaction of the electric field with the fluid flow combines and extends standard methods for time and space discretization. We require a stable method to obtain approximate solutions to the system (29a, 29b), (32). To simplify the presentation, a domain setup as in Fig. 2 is used. However, the developed simulation method is applicable to general domains with the traveling wave boundary may be induced by arbitrarily shaped electrodes.

We treat the complete system as a Navier–Stokes problem with a volume force influence on the momentum. This force is computed from (33) using the solution of system (32).

For advancing the incompressible Navier–Stokes equations in time, the so-called splitting methods introduced by (Chorin 1968; Patankar 1972) are suitable. A recent overview of these methods can be found in (Guermond et al. 2006). For the space discretization finite volume (FV) methods are a convenient choice, we use the discretizations from Ferziger (1996, Chapter 7).

Because the equations depend on time and space, we are dealing with an initial and boundary value problem. The potential system (32) implicitly depends on time through the dependence of the electrical conductivity on temperature. We simplify the equations by replacing this time dependence from the potential system for the numerical simulation by a linear, space-dependent approximation for the electrical conductivity for our experimental comparison in Sect. 5.

4.1 Initial and boundary conditions

Initial conditions are needed for the unknown velocity $\mathbf{u}$, pressure p and the potentials Φ_c, Φ_s. The system of potential (32) is elliptic, therefore, the solution depends only on the boundary conditions and is hence independent of the initial conditions. We initialize the potential fields with 0. Without an electric field, no forces act on the fluid and hence the momentum of the fluid is also initialized with 0. As there are no external forces other than that from the electrical field, we assume that the pressure initially is constant in space inside the domain and we fix it to 0.

As the traveling wave boundary condition on the top boundary of the domain for our experimental comparison setup in Sect. 5, we use the condition given in Eq. (5) with $\mathbf{k}$ pointing in x direction and $\mathbf{r}$ spanning the whole top boundary.

In our numerical test, the dielectric function ε is assumed to be constant. Only the electric conductivity exhibits a spatial variation. In general, this variation is due to a temperature dependence. Temperature variations are in most applications implicitely induced by the averaged Joule heating term, Eq. (35). This makes the system for the electrical potentials (32) implicitely time dependent and strongly coupled to the Navier–Stokes system (29a, 29b). In Böttcher et al. (2011), this coupled system was solved and compared with experiments. For the test of the numerical algorithm, we assume that the temperature T varies linearly between bottom and top, which yields in leading order a linear variation of the conductivity σ.

4.2 The discretization

The systems (32), (29a, 29b) are discretized in space by cell-centered finite volumes. Let the domain Ω be partitioned into a set of N volumes $\{\mathbf{V}_k, k = 0 \ldots N-1\}$ of cuboid shape such that $\Omega = \sum_{k=0}^{N-1} \mathbf{V}_k$.

Let us exemplify the FV discretization for Eq. (29a). It is derived by integrating the PDE over each volume $\mathbf{V}_k$. For ease of notation, let $\mathbf{V}$ be any fixed volume $\mathbf{V}_k$.

$$\int_{\mathbf{V}} (\partial_t(\rho u_i) + \partial_j(\rho u_i u_j) + \partial_i p - \langle \rho_e E_i \rangle^t - \eta \partial_j^2 u_i) \mathrm{d}x\mathrm{d}y\mathrm{d}z = 0. \quad (36)$$

This volume integral is then transformed to surface integrals over the enclosing surfaces of the volume $\mathbf{V}$ where the Gauss theorem is applicable. Otherwise, the volume integral is approximated by multiplying the volume V of the cuboid with the value of the field at the midpoint of the cuboid. Hence, for each PDE, we obtain N ODEs with only the time derivative remaining in each.

$$V\partial_t(\rho u_i) + \int_{\partial \mathbf{V}} (\rho u_i \mathbf{u}) \cdot \mathbf{n} \mathrm{d}S + V\partial_i p - \int_{\mathbf{V}} (\langle \rho_e E_i \rangle^t) \mathrm{d}V - \eta \int_{\partial \mathbf{V}} (\partial_j u_i n_j) \mathrm{d}S = 0. \quad (37)$$

The approximations of the surface integrals in the second and fifth term of (37) are standard, first-order

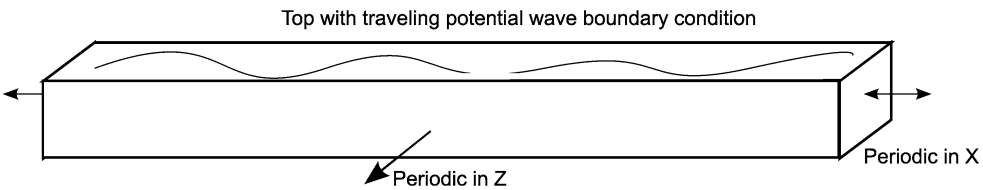

Fig. 2 The simulation domain with the traveling wave boundary condition on *top*. The boundaries in x direction and z direction are periodic

approximations of values and gradients on the surface midpoints of the cuboid and can be found, e.g. in (Ferziger 1996). Let us introduce operators for the discrete divergence and gradient in finite volume discretization $\mathcal{DIV}$ and $\mathcal{G}$. The FV discretizations of the other equations (29b) and (32) are then straightforward using the same method and will not be given in detail here.

In time, the equations are discretized on a mesh of timesteps $\{t^n, n \in \mathbb{N}, n > 0\} \subset [0, T] \subset \mathbb{R}$ using implicit Euler discretization. We advance the system (32), (29a, 29b) in time by substeps. First, we obtain a potential from (32). The solution of this homogeneous elliptic system only depends on the boundary conditions, i.e. the traveling wave prescribed on parts of the domain and given in (5). Hence this solution needs to be computed only once and does not need to be recomputed in later time steps.

Then, for the solution of the incompressible Navier–Stokes system (29a, 29b), we introduce intermediate discrete times within each discrete time interval $[t^n, t^{n+1} = t^n + \tau]$ denoted by $t^{n+\alpha}$ with $0 < \alpha < 1$.

So let us assume a constant density ρ and that the pressure p^n is known from the previous discrete moment in time. To obtain a first guess of the velocity in the current time step, we solve the discretized integral form of the momentum equation (29a) in componentwise form, given here for any volume $\mathbf{V}$:

$$\frac{V}{\tau}\left[(\rho u)_i^{n+\frac{1}{2}} - (\rho u)_i^n\right] + \mathcal{DIV}((\rho u)_i^{n+\frac{1}{2}}\mathbf{u}^n) + V\mathcal{G}_i(p^n) - \eta\mathcal{DIV}((\mathcal{G}u_i^{n+\frac{1}{2}})) = \int_{\mathbf{V}} (\langle \rho_e E_i \rangle^t) dV, \tag{38}$$

with $(\rho u)^{n+\frac{1}{2}}$ and $i = 1, \ldots, 3$, where the gradient in the last term of the left side is computed on the midpoints of the faces and the convective term is linearized. Let us moreover assume that all other changes in velocity are induced by the gradient of the pressure correction, then we reach the following condition for the corrected velocity and pressure

$$\frac{V}{\tau}\left[(\rho u)_i^{n+1} - (\rho u)_i^{n+\frac{1}{2}}\right] = -V\mathcal{G}_i(p^{n+1} - p^n),$$
$$i = 1, \ldots, d \Leftrightarrow (\rho\mathbf{u})^{n+1} = (\rho\mathbf{u})^{n+\frac{1}{2}} - \tau\mathcal{G}_{\mathcal{F}}(p') \tag{39}$$

where $p' := p^{n+1} - p^n$. We apply the discrete divergence $\mathcal{DIV}(\cdot)$ to (39). Then, with the discretized equation (29b)

$$\mathcal{DIV}(\rho^{n+1}\mathbf{u}^{n+1}) = 0$$

we transform (39) into an elliptic equation for the correction to the pressure p'

$$\tau\mathcal{DIV}(\mathcal{G}(p')) = \mathcal{DIV}(\rho^{n+\frac{1}{2}}\mathbf{u}^{n+\frac{1}{2}}) \tag{40}$$

for the unknown p' which is an elliptic equation. Hence, we have transformed the solution of one-time step into two steps of solving the linearized velocity equation (38) and the solution of a second order PDE (40) with a Laplace operator. We summarize the steps into the Algorithm 1.

Algorithm 1: Simulation of electric force induced fluid flow

```
Solve discretized version of system (32);
Compute discrete version of f by (33) at time t = 0;
t^n = 0;
while Steady state has not been reached do
    t^{n+1} = t^n + τ, with timestep τ;
    Solve linearized momentum prediction (38) for (ρu)^{n+1/2} with old pressure;
    Solve pressure correction equation (40) for p';
    Correct momentum to (ρu)^{n+1} using (39);
    p^{n+1} = p^n + p';
```

5 Experimental comparison

In this section, we check the derived equations and numerical implementation against the results from (Melcher 1967). Let us state the parameters used. As traveling wave boundary condition, a sinusoidal potential with $k = 2\pi/h_x = 7.08\,\frac{1}{\mathrm{m}}$ is chosen according to the experimental wavelength $h_x = 0.89m$. The specific forms and values of $\varepsilon, \sigma, \omega$ and η match the values from Melcher (1967) where the fluid was corn oil with a density of $\rho = 921\,\mathrm{kg/m^3}$. The relative permittivity for corn oil used in Melcher (1967) is $\varepsilon = 3.1$. We estimate from Melcher (1967, Figure 5) that the temperature at the bottom is 15 °C and at the top 38 °C. The electric conductivity is then given by $\sigma(y) = \sigma(0) + \sigma_1\frac{y}{h_y}, \sigma_1 = \sigma(h_y) - \sigma(0)$, cf. (Melcher 1967, Paragraph 2, p. 1180). The conductivity constants are $\sigma(0) = 2.95 \times 10^{-11}\,\frac{\mathrm{S}}{\mathrm{m}}$ and $\sigma_1 = 7.9 \times 10^{-11}\,\frac{\mathrm{S}}{\mathrm{m}}$ as in Melcher (1967, Table 1). The traveling wave frequency ω is $0.4 \cdot 2\pi\,\frac{1}{\mathrm{S}}$. The flow occurs in a channel as depicted in Fig. 2 where the height of the channel h is 3×10^{-2} m and the length is 0.88 m. Results of the simulation with these parameters are displayed in Fig. 3.

For quantitative comparison, we rely on (Melcher 1967, Figures 6,8, p. 1183). Experimental (Melcher 1967, Figure 6, p. 1183) and numerical flow profile for a peak potential of 8.25×10^3 V exhibit nearly perfect agreement as shown in Fig. 3. Furthermore, in Melcher (1967 Figure 8, p. 1183), the peak velocity over the square of the experimental potential signal is displayed. The experimental signal is a complicated superposition of many frequencies, where the amplitude of the lowest frequency is the main driving force for the traveling wave (Melche 1966). Since we assume a sinusoidal wave, our amplitude of 8.25×10^3 V corresponds roughly to an experimental peak potential of 12.5×10^3 V (Melcher 1967). The peak velocity at this value in Melcher (1967, Figure 8, p. 1183) is about $0.45\,\frac{\mathrm{cm}}{\mathrm{S}}$. The peak velocity in our simulation (see

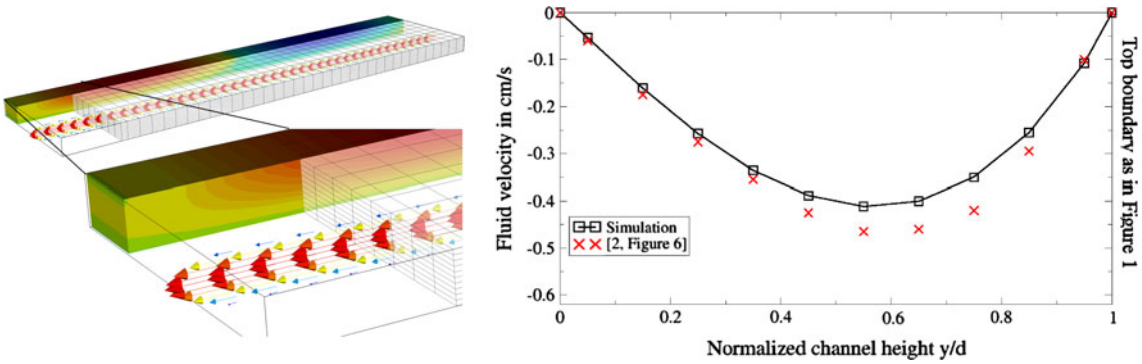

Fig. 3 *Left* three-dimensional plot of induced channel flow depicting the sine component of the potential by the *pseudocolor*, the spatial resolution of the mesh and a slice of the velocity profile as arrows colored by magnitude. *Right* profile of absolute x velocity from the bottom of the channel to the *top* of the channel (*left* to *right* on the x axis) through the channel center for an amplitude of 8.25×10^3 V

Fig. 3) of $0.4116 \frac{\text{cm}}{\text{s}}$ is within the experimental error of the measurements. The slightly lower numerical value may be explained by the small contribution of higher frequencies in the experimental voltage to the effective force.

The temperature dependence of the viscosity of corn oil is given in Melcher (1967, Table 1, Figure 5) and assumed to vary between 7.5×10^{-2} and 2.57×10^{-2} Pa s.[1] As can be seen in the numerical simulation, this dependence of the viscosity is responsible for the off-centering of the velocity peak in the y profile in Fig. 3. With constant viscosity, the induced flow shows a close to ideal Hagen–Poiseuille profile.

6 Conclusion

Using a standard thermodynamic approach (Landau 1984; Liu 1993; Jiang 1996), we have rederived the time averaged, thermodynamic consistent equations for electrohydrodynamical flows induced by high frequency electromagnetic fields. The equations can be applied to electroosmotic and electrothermally induced flows. We concentrated on the latter for validation purposes. A numerical scheme was developed and implemented which allows efficient, spatially fully resolved simulations of the electrothermally induced flows and the electric fields at arbitrary frequencies within the range of validity of the model, mainly given by (12) and (14). The shape of the electrodes and shape of the channel can be arbitrarily chosen. Furthermore, because of the time averaging procedure, all regimes from clear separation of hydrodynamic and electric field time scales to no scale separation can be simulated. Time variations of the fluid flow on the scale of electric field alternation will of course not be reproduced because of the averaging. The range of applications and the real-world applicability in microchannels have already been demonstrated in a much more involved test in (Böttcher et al. 2011). There, temperature and convective particle transport were additionally taken into account. With this current paper, we deliver the missing derivation of the model and the numerical method. For validation of the method, we compare our simulations with the experimental results in (Melcher 1967). Within experimental errors, mainly related to the mapping of the complex experimental voltage signal to the one used in the numerical simulations, experiment and simulation show perfect agreement.

In conclusion, the numerical implementation of the model offers the possibility to study spatially complex electromagnetically driven flows in all applications where the penetration depth of the electric field is comparable or bigger than the experimental setup and where dissipation and dispersion of the electromagnetic field can be neglected.

[1] Note that the table and the figure in the reference contradict each other in values of the minimum viscosity, we have assumed the figure to be correct.

References

Böttcher M, Schmidt S, Latz A, Jäger S, Stuke M, Duschl C (2011) Filtration at the microfluidic level: enrichment of nanoparticles by tuneable filters. J Phys Condens Matter 23(32): 324101. doi: 10.1088/0953-8984/23/32/324101., http://stacks.iop.org/0953-8984/23/i=32/a=324101

Chorin AJ (1968) Numerical solution of Navier–Stokes equation. Math Comput 22:745–760

Felten M, Geggier P, Jäger M, Duschl C (2006) Controlling electrohydrodynamic pumping in microchannels through defined temperature fields. Phys Fluids 18:051,707

Felten M, Staroske W, Jäger S, Schwille P, Duschl C (2008) Accumulation and filtering of nanoparticles in microchannels using electrohydrodynamically induced vortical flows. Electrophoresis 29:2987–2996

Ferziger JH, Perić M (1996) Computational methods for fluid dynamics. Springer

Fuhr G, Hagedorn R, Muller T, Benecke W, Wagner B (1992) Microfabricated electrohydrodynamic (EHD) pumps for liquids of higher conductivity. J Microelectromech Syst 1(3):141–146. doi:10.1109/84.186393

Fuhr G, Schnelle T, Wagner B (1994) Traveling wave-driven microfabricated electrohydrodynamic pumps for liquids. J Micromech Microeng 4:217–226

Green NG, Ramos A, Gonzalez A, Morgan H, Castellanos A (2002) Fluid flow induced by nonuniform ac electric fields in electrolytes on microelectrodes. III Observation of streamlines and numerical simulations. Phys Rev E 66:026,305

Green NG, Ramos A, Morgan H (2000) Ac electrokinetics: a survey of sub-micrometre particle dynamics. J Phys D Appl Phys 33:632–641

Guermond JL, Minev PD, Shen J (2006) An overview of projection methods for incompressible flows. Comput Methods Appl Mech Eng 195:6011–6045

Iverson D, Cremaschi L, Garimella V (2009) Effects of discrete-electrode configuration on traveling-wave electrohydrodynamic pumping. Microfluid Nanofluid 6(2):221–230

Jiang Y, Liu M (1996) Dynamics of dispersive and nonlinear media. Phys Rev Lett 77:1043–1046

Landau LD, Lifshitz EM (1984) Electrodynamics of continuous media. Pergamon Press, Oxford

Liu M (1993) Hydrodynamic theory of electromagnetic fields in continous media. Phys Rev Lett 70:3580–3583

Melcher JR (1966) Traveling-wave induced electroconvection. Phys Fluids 9:1548–1555

Melcher JR, Firebaugh MS (1967) Traveling-wave bulk electroconvection induced across a temperature gradient. Phys Fluids 10(6):1178–1185. doi:10.1063/1.1762260, http://link.aip.org/link/?PFL/10/1178/1

Patankar SV, Spalding DB (1972) A calculation procedure for heat, mass and momentum. Int J Heat Mass Transf 15:1787–1806

Ramos A, Morgan H, Green N.G, Castellanos A (1998) Ac electrokinetics: a review of forces in microelectrode structures. J Phys D Appl Phys 31:2338–2353

Russel WB, Saville DA, Schowalter WR (1989) Colloidal dispersions. Cambridge monographs on mechanics and applied mathematics. Cambridge University Press, Cambridge